The 2025 World Congress on
Advances in Structural Engineering and Mechanics (ASEM25)
BEXCO, Busan, Korea, August 11-14, 2025

Characterization of discontinuities within stiff surface layers using non-destructive techniques

*Eun Sang Lee[1)], Heechang Hwang[2)] and Won-Taek Hong[3)]

[1), 2), 3)] *Department of Civil & Environmental Engineering, Gachon University, 1342, Seongnam-daero, Gyeonggi-do, 13120, Republic of Korea*
[1)] *dldmstkd20@gachon.ac.kr*

ABSTRACT

To investigate discontinuities in stiff surface layers, traditional invasive techniques such as coring and drilling have been adopted, which may significantly disturb and destabilize the target grounds or construction materials. In this study, non-destructive technique using electromagnetic wave is employed to characterize discontinuities within a stiff layer. To simulate the stiff layers and four types of discontinuities, two blocks made of cementitious material were prepared, with the space between them filled with air, water, dry sand, and saturated sand. Electromagnetic wave was transmitted, and that reflected from the simulated discontinuities was measured on one side of the block. The experimental results show that the depth of the discontinuities, estimated from the travel time of the wave, corresponds to the thickness of the block. In addition, the electromagnetic properties of the materials filling the space can be estimated using the amplitude ratios of the reflected wave to the transmitted wave, known as reflection coefficients. This study demonstrates that non-destructive techniques using electromagnetic wave can be an effective surveying method to characterize discontinuities in stiff layers.

1. INTRODUCTION

With the increasing concentration of population in urban areas, the demand for the construction of transportation infrastructure and the development of underground spaces has been steadily rising, with the aim of making efficient use of limited land resources. To ensure the stable behavior and durability of such infrastructures, the ground surface is reinforced and protected using stiff materials, such as cementitious materials (Bernard 2020). When anomalies such as cracks or loosened zones develop within these stiff layers or in the adjacent ground, they may induce rapid deformation and brittle failure of the infrastructure, potentially resulting in significant loss of life and property (Kao 2025).

[1)] Graduate Student
[2)] Graduate Student
[3)] Associate Professor

However, due to the high rigidity of these stiff layers, there are inherent limitations in visually observing early signs of anomalies within the cementitious materials or in the adjacent grounds.

For the investigation of discontinuities within stiff surface layers, traditional invasive methods such as coring and drilling can be employed, and these methods have also been used for the assessment of the integrity of backfill grouting materials behind linings (Ye 2020). Although invasive methods provide relatively objective and accurate results, they may cause disturbance (Holt 2000) and permanent deformation to the target infrastructure (Si 2025), and are inefficient in terms of both cost and time (Hasan 2021). Therefore, the application of non-destructive geophysical surveying techniques is required to enable efficient investigation over a wide area while minimizing disturbance to the target infrastructure.

Ground penetrating radar (GPR), one of the most commonly used geophysical surveying methods, detects the depth of interfaces between layers with different electromagnetic properties (Galagedara 2005, Tallini 2004) and is effective for non-ferromagnetic materials with low electromagnetic energy absorption, such as fully cured cementitious materials and geo-materials (Arosio, 2016). In particular, GPR survey requires significantly less physical space during operation compared to other geophysical surveying methods such as electrical resistivity survey and seismic wave survey, which allows for efficient application even in environments with strict spatial and temporal constraints (Kiflu 2016). Moreover, since no additional surface-mounted sensors are required, GPR is well-suited for use on stiff surface layers (Hong 2018). In the case of applications of GPR survey to investigate the discontinuities within stiff surface layers, the evaluation of material characteristics composing the discontinuities is a critical factor to assess the potential risks to infrastructures as well as the localization of discontinuities based on interface depth (Grégoire 2004).

In this study, discontinuities composed of four different materials were prepared within stiff layers simulated by using cementitious materials, and electromagnetic waves were collected through GPR surveys conducted on the surface of the stiff layers. This paper describes the theoretical background and considerations of GPR surveys, the experimental setup and results, and discusses the characteristics of the electromagnetic waves obtained under various experimental conditions.

2. GROUND PENETRATING RADAR (GPR)

2.1 Measurement system

In the geotechnical practices, ground penetrating radar (GPR) system is used to determine the depth of the interfaces between layers that have different electromagnetic properties (Yu 2023). Typical GPR system consists of an antenna and a control unit (Daniels 2004). The antenna has two dipoles at its base: transmitter (TX) and receiver (RX) as illustrated in Fig. 1. The electromagnetic wave emitted from the TX propagates in Medium 1 and is partially reflected at the interface between Media 1 and 2, and the reflected electromagnetic wave is collected by the RX as also shown in Fig. 1. The reflected electromagnetic wave is recorded on a temporal scale, thus the velocity of the electromagnetic wave (v) in Medium 1 is

$$v = \frac{c}{\sqrt{\varepsilon_r}} = \frac{S}{\Delta t} \tag{1}$$

where ε_r is the relative permittivity of the Medium 1; v and c are the velocities of the electromagnetic wave in the Medium 1 and in a vacuum (2.998×10^8 m/s), respectively. S and Δt denote the roundtrip travel distance and travel time of the electromagnetic wave, respectively. Therefore, interface depth (d) from the surface can be calculated as

$$d = \frac{S}{2} = \frac{c\Delta t}{2\sqrt{\varepsilon_r}} \tag{2}$$

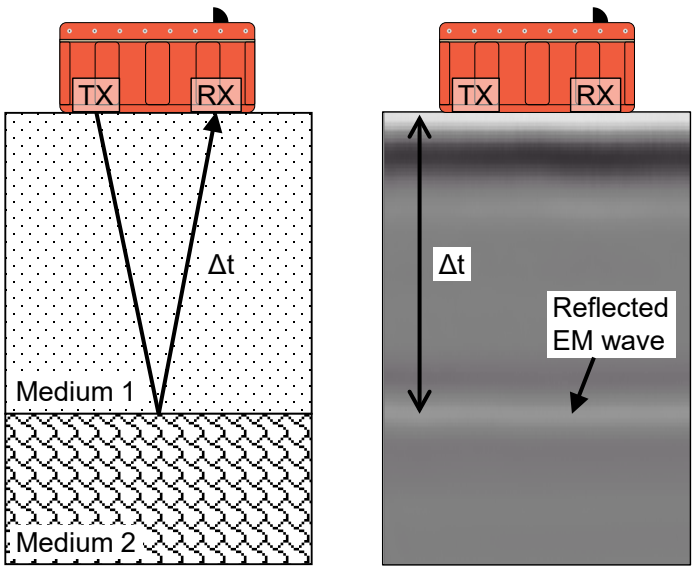

Fig. 1 Ground penetrating radar (GPR) system

2.2 Reflection characteristics of electromagnetic wave

When the electromagnetic wave emitted from the GPR antenna encounters an interface, it is partially reflected according to the reflection coefficient (R^*), which is defined as an amplitude ratio between the reflected and incident electromagnetic waves at the interface. The reflection coefficient is calculated as Eq. (3) (Santamarina 2001).

$$R^* = \frac{z_2^* - z_1^*}{z_2^* + z_1^*} \tag{3}$$

where z^*_1 and z^*_2 are the electromagnetic impedances of Media 1 and 2, respectively. The electromagnetic impedance (z^*) in a medium is defined as the relative variation of the electric field and the magnetic field and is calculated as Eq. (4).

$$z^* = \frac{c}{\sqrt{\varepsilon_r - j\left\{\varepsilon' + \sigma/\left(f\varepsilon_0\right)\right\}}}\mu_0 \tag{4}$$

where j represents an imaginary number, ε′ denotes the out-of-phase component of permittivity, σ indicates the electrical conductivity of the medium, and ε_0 and μ_0 are the permittivity and magnetic permeability in a vacuum, respectively. For non-ferromagnetic materials, including fully cured cementitious materials and most geo-materials, both ε′ and σ are assumed to be zero. Consequently, in these conditions, the electromagnetic impedance (z*) can be simplified to Eq. (5).

$$z^* = \frac{c}{\sqrt{\varepsilon_r}}\mu_0 \tag{5}$$

Because the velocity of the electromagnetic wave (c) and the magnetic permeability (μ_0) in a vacuum are constant, the electromagnetic impedance is inversely proportional to the square root of the relative permittivity. Therefore, the relative permittivity relationship between Media 1 and 2 can be evaluated based on the polarity changes of the reflected electromagnetic wave as illustrated in Fig. 2, and the relative permittivity of the discontinuities can be estimated based on amplitude of the reflected electromagnetic waves (Van der Meer 2004).

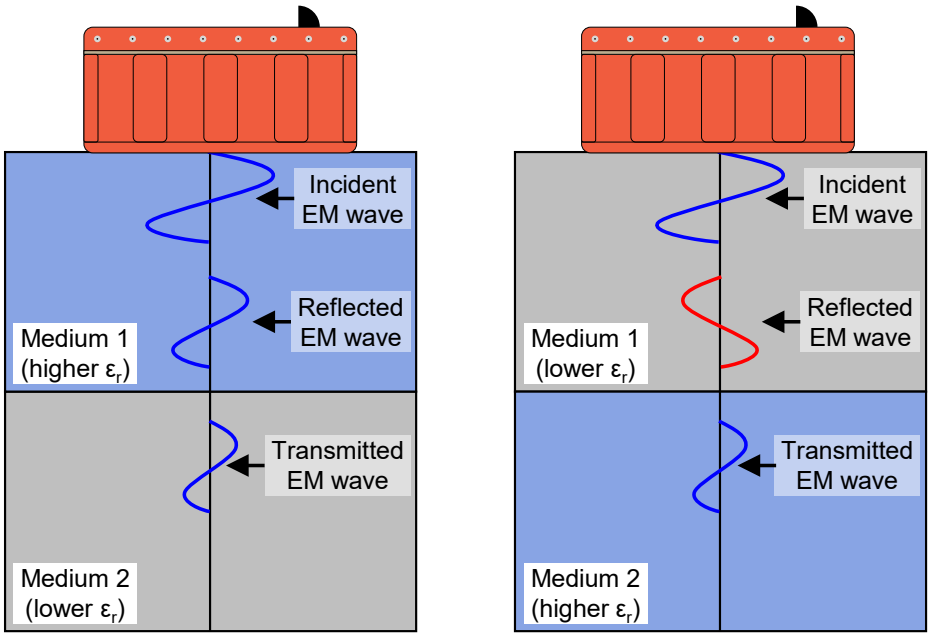

$\varepsilon_{r1} > \varepsilon_{r2}$, $Z_1^* < Z_2^*$, $R^* > 0$ $\varepsilon_{r1} < \varepsilon_{r2}$, $Z_1^* > Z_2^*$, $R^* < 0$

Fig. 2 Reflection characteristics of electromagnetic waves

3. EXPERIMENTAL STUDY

3.1 Experimental setup

For the simulation of the discontinuities within stiff layers, two cementitious specimens were prepared each with a width and length of 600 mm, and thicknesses of

100 mm and 200 mm, respectively, and four different materials (air, dried sand, saturated sand, and water) were filled between the specimens as illustrated in Fig. 3.

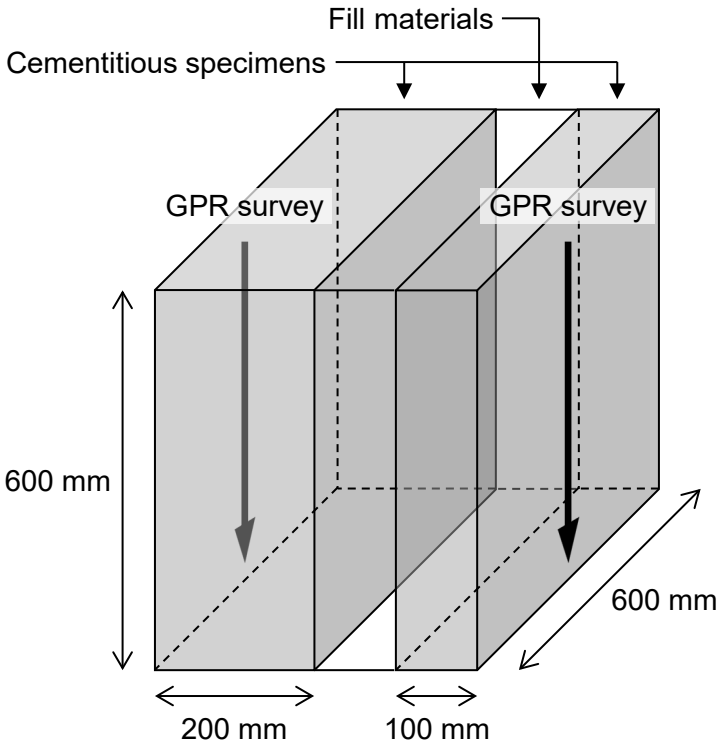

Fig. 3 Experimental setup

GPR surveys were conducted on both surfaces of the cementitious specimens using a GPR system with a center frequency of 2.7 GHz (Mini LXT, Geophysical Survey Systems Inc.). A bandpass filter was applied to eliminate high-frequency noise above 3 GHz and low-frequency noise below 1.7 GHz. Note that the relative permittivity (ε_r) values of the cementitious specimen, and the fill material, measured using a time domain reflectometry (TDR) system, are summarized in Table 1.

Table 1 Relative permittivity of used materials

Material	Relative permittivity
Cementitious specimen	7.14
Air	1
Dried sand	2.32
Saturated sand	29.35
Water	79.63

3.2 Experimental results

The GPR images and signals obtained for various materials filled between the cementitious specimens are presented in Fig. 4. Fig. 4(a) and Fig. 4(b) show the GPR images and corresponding signals acquired from the surfaces of specimens with thicknesses of 100 mm and 200 mm, respectively. In both cases, signals reflected from

the specimen surface and from the interface between the specimen and the fill material were clearly identified through the GPR survey. To enhance the visual clarity of the acquired signals, a gain of 27 dB was applied to the surface reflection signals, while gains of 30 dB and 40 dB were applied to the signals reflected from the interfaces between the fill material and the specimens of 100 mm and 200 mm thickness, respectively.

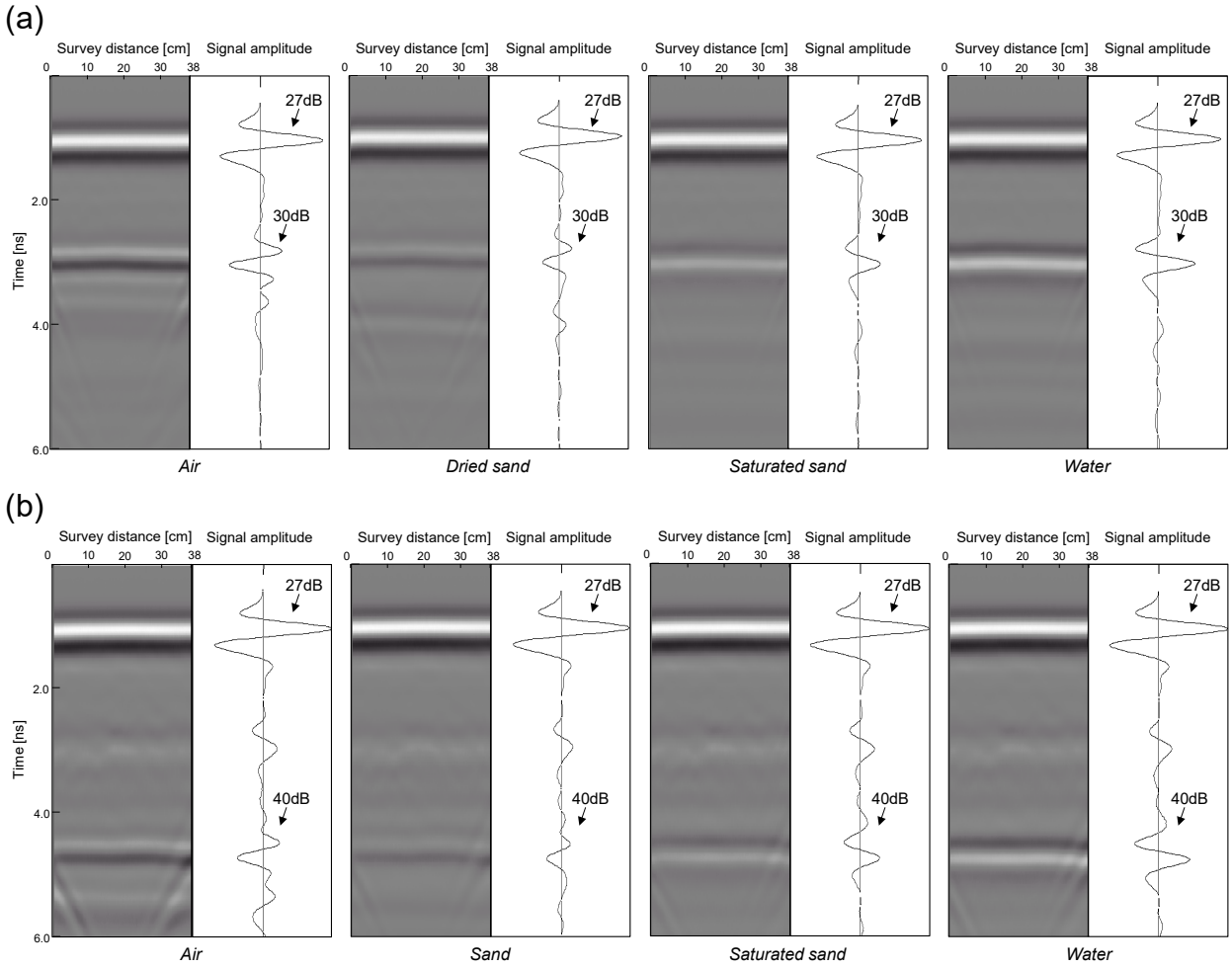

Fig. 4 GPR images and signals acquired from the surface of cementitious specimens with different thicknesses: (a) 100 mm; (b) 200 mm

At the surface of the cementitious specimens, the reflected electromagnetic wave exhibited a reversal polarity to that of the wave emitted from the transmitter (TX). Accordingly, when fill materials with lower relative permittivity than the cementitious specimen, such as air and dry sand, were used, the reflected signals at the interface showed reversal polarity to the surface reflection signal. Conversely, when fill materials with higher relative permittivity, such as saturated sand and water, were used, the interface reflection signals exhibited the same polarity as the surface reflection. Additionally, even when the reflected signals exhibited the same polarity, such as in the cases of air and sandy soil, or saturated sandy soil and water, a greater the difference in

relative permittivity between the cementitious specimen and the fill material resulted in a higher amplitude of the reflected signal.

4. ANALYSES AND DISCUSSION

4.1 Reflection characteristics according to types of discontinuities

An example of GPR signal is presented in Fig. 5. The electromagnetic wave emitted from the TX is partially reflected at both the surface of the cementitious specimen and the interface between the specimen and the fill material. The amplitudes of the signals reflected at the surface and the interface are defined as A_s and A_i, respectively. For the quantitative comparison and analysis of the signals reflected from the cementitious specimen–fill material interfaces (Fig. 4), the interface amplitude was normalized by the surface amplitude to calculate the normalized amplitude ($A_n = A_i/A_s$). Note that, for objectivity in the calculation of A_n for all collected signals, gain values applied in Fig. 4 were removed from the data.

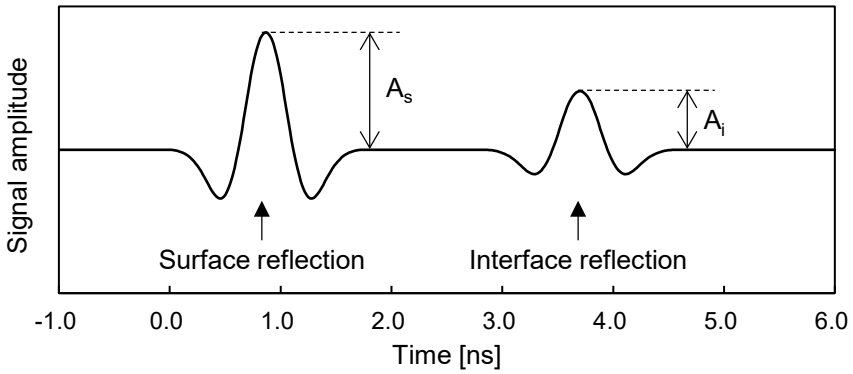

Fig. 5 Determination of normalized amplitude using surface and interface reflections

Normalized amplitudes of GPR signals reflected from various fill materials, determined on the surfaces of cementitious specimens with thicknesses of 100 mm and 200 mm are plotted in Figs. 6(a) and 6(b), respectively, with their reflection coefficients (R^*) at the interfaces. When the thickness of the cementitious specimen was 100 mm, the normalized amplitudes (A_n) were determined to be -0.353, -0.188, 0.248, and 0.419 for air, dried sand, saturated sandy soil, and water, respectively. In the case of the 200 mm-thick specimen, the corresponding A_n values were -0.084, -0.049, 0.062, and 0.102, respectively. To determine the R^* at the interface for each case, the electromagnetic impedances (z^*) of the materials used in this study were calculated using the relative permittivity values summarized in Table 1 along with Eqs. (4) and (5). These calculated z^* values were then substituted into Eq. (3). Thus, R^* values at the interface between the cementitious specimen and the air, dried sand, saturated sand, and water were determined to be 0.455, 0.273, -0.339, and -0.537, respectively.

As described in Eqs. (4) and (5), the z^* is inversely proportional to the square root of relative permittivity, and the R^* is proportional to the difference in z* values at the interface. Therefore, the greater the difference in relative permittivity between the cementitious specimen and the fill material, the higher the energy of the electromagnetic wave reflected at the interface as shown in Fig. 6. In addition, since the signal reflected

from the surface of the cementitious specimen used for calculating A_n has the opposite polarity to that of the electromagnetic wave emitted from the TX, the signs of A_n and R^* are opposite, resulting in a negative coefficient in the relationships between A_n and R^*.

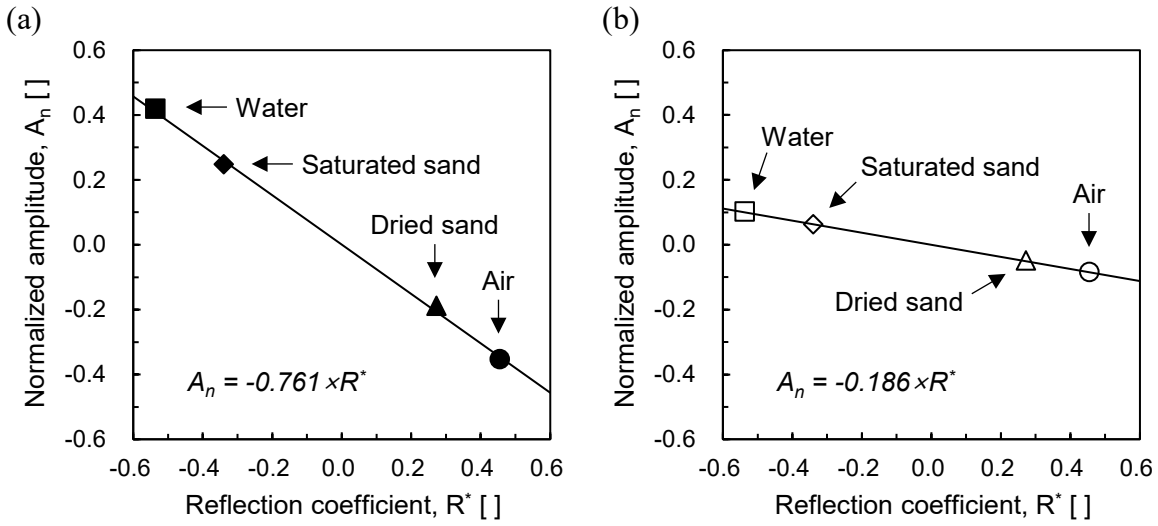

Fig. 6 Normalized amplitudes of signals reflected from fill materials, determined on the surfaces of cementitious specimens with different thicknesses: (a) 100 mm; (b) 200 mm

4.2 Energy attenuation due to depth of discontinuities

The energy of transmitted and reflected waves propagating through a medium continuously attenuates during propagation. In this study, cementitious specimens with thicknesses of 100 mm and 200 mm were used. As the wave propagation distance doubled, the amplitudes of the reflected signals collected at the interface for air, dried sand, saturated sand, and water, respectively, decreased to 23.8%, 26.0%, 25.3%, and 24.4% of their original values, as shown in Fig. 7, resulting in an average reduction of approximately 24.8%. This is consistent with the theoretical attenuation ratio of energy for radially propagating electromagnetic waves (Neto 2006), which is also reflected in the correlation coefficients between A_n and R^* in Figs. 6(a) and 6(b).

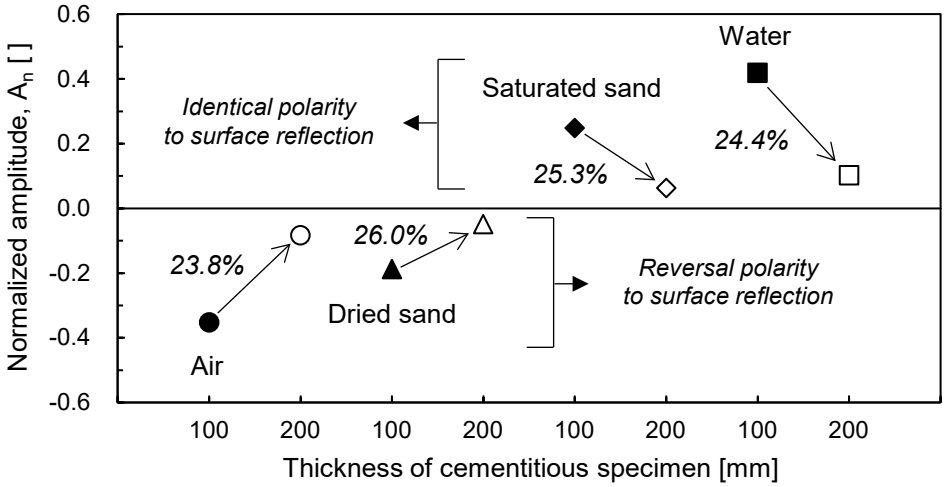

Fig. 7 Attenuation ratio of reflected electromagnetic waves

5. SUMMARY AND CONCLUSIONS

In this study, the materials existing behind stiff layers were characterized by analyzing the amplitude and polarity of reflected electromagnetic (EM) waves obtained from ground penetrating radar (GPR) surveys. To measure the amplitude of EM waves reflected at the interface between materials with different electromagnetic impedances, cementitious specimens with thicknesses of 100 mm and 200 mm were prepared. Four types of fill materials, such as air, dried sand, saturated sand, and water, with different electromagnetic properties were placed between the specimens. GPR surveys were conducted on both surfaces of the cementitious specimens, and normalized amplitudes (A_n) were calculated using the surface and interface reflection signals and comparatively analyzed.

The greater the difference in relative permittivity and electromagnetic impedance between the propagating medium (cementitious specimen) and the fill material forming the discontinuity, the larger the reflected EM energy. However, the signal reflected at the surface of the cementitious specimen has a reversal polarity to the EM wave emitted from the transmitter (TX), resulting in opposite signs between A_n determined at the surface and the reflection coefficient (R^*) calculated at the interface. Therefore, a negative correlation between A_n and R^* was observed.

Since EM waves attenuate continuously during propagation within a medium, the A_n values determined at the surfaces of specimens with different thicknesses vary, even for interfaces with the same material combination. As observed in this study, when the thickness of the propagation medium was doubled, the amplitude of the reflected signal measured at the cementitious surface decreased by approximately 24.8%, indicating an attenuation ratio inversely proportional to the square of the wave propagation distance. This study investigated the reflection characteristics of EM waves based on the thickness of the surface layer and the type of fill material. Therefore, the analytical methodology suggested in this study is expected to be applicable for identifying discontinuities within stiff surface layers based on the electromagnetic properties of the surface materials and the collected GPR signals reflected from the surface and internal interfaces.

ACKNOWLEDGEMENT

This work was supported by the National Research Foundation of Korea (NRF) grant funded by the Korea government (MSIT) (RS-2024-00337686).

REFERENCES

Arosio, D. (2016), “Rock fracture characterization with GPR by means of deterministic deconvolution”, *J. Appl. Geophy.*, **126**, 27–34.

Bernard, E. S. and Thomas, A. H. (2020), “Fibre reinforced sprayed concrete for ground support”, *Tunn. Undergr. Space Technol.,* **99**, 103302.

Daniels, D. J. (Ed.). (2004), Ground penetrating radar (2nd ed.), The Institution of Engineering and Technology, Stevenage, U.K.

Galagedara, L. W., Redman, J. D., Parkin, G. W., Annan, A. P. and Endres, A. L. (2005), "Numerical modeling of GPR to determine the direct ground wave sampling depth", *Vadose Zone J.,* **4**(4), 1096-1106.

Grégoire, C. and Hollender, F. (2004), "Discontinuity characterization by the inversion of the spectral content of ground penetrating radar (GPR) reflections—Application of the Jonscher model", *Geophysics*, **69**(6), 1414–1424.

Hasan, M., Shang, Y., Meng, H., Shao, P. and Yi, X. (2021), "Application of electrical resistivity tomography (ERT) for rock mass quality evaluation", *Sci. Rep.*, **11**(1), 23683.

Holt, R. M., Brignoli, M. and Kenter, C. J. (2000), "Core quality: quantification of coring-induced rock alteration", *Int. J. Rock Mech.,* **37**(6), 889-907.

Hong, W.T., Kang, S., Lee, S.J. and Lee, J.S. (2018), "Analyses of GPR signals for characterization of ground conditions in urban areas", *J. Appl. Geophy.*, **152**, 65–76.

Kao, S., Zhao, G., Meng, X., Dong, C. and Huang, S. (2025), "Influences of slurry properties on the mechanical properties and failure mode of broken rock consolidated body", *J. Mech. Sci. Technol.*, **39**(6), 3155–3166.

Kiflu, H., Kruse, S., Loke, M.H., Wilkinson, P.B. and Harro, D. (2016), "Improving resistivity survey resolution at sites with limited spatial extent using buried electrode arrays", *J. Appl. Geophys.*, **135**, 338–355.

Neto, P. X. and de Medeiros, W. E. (2006), "A practical approach to correct attenuation effects in GPR data", *J. Appl. Geophy.,* **59**(2), 140-151.

Santamarina, J.C., Klein, K. A. and Fam, M.A. (2001), Soils and Waves: Particulate Materials Behavior, *Characterization and Process Monitoring*, John Wiley and Sons, NY.

Si, X., Meng, Q., Pan, G., Zhang, X., Li, G., Li, Z. and Wang, P. (2025), "Progressive strategies of single-channel seismic survey for geological characterization assessment in urban areas", *J. Geophys. Eng.*, **22**(3), 774–784.

Tallini, M., Giamberardino, A., Ranalli, D. and Scozzafava, M., "GPR survey for investigation in building foundations", *Proceedings of the Tenth International Conference on Grounds Penetrating Radar, 2004. GPR 2004,* Delft.

Van der Meer, W. P. J., and Inoue, Y. (2004), "Using interference to determine the phase change of a reflected GPR pulse"*, Proceedings of the Tenth International Conference on Grounds Penetrating Radar, 2004. GPR 2004,* Delft.

Ye, Z. and Zhang, C. (2020), "Influence of loose contact between tunnel lining and surrounding rock on the safety of the tunnel structure", Symmetry, **12**(10), 1733.

Yin, L., Zhang, Y., Dai, L., Zhang, J., Li, J. and Yang, C. (2023), "Quantitative study of the weakening effect of drilling on the physical and mechanical properties of coal–rock materials", *Materials*, **16**(19), 6424.

Yu, Q., Li, Y., Luo, T., Zhang, J., Tao, L., Zhu, X., Zhang, Y., Luo, L. and Xu, X. (2023), "Cement pavement void detection algorithm based on GPR signal and continuous wavelet transform method", *Sci. Rep.*,**13**(1), 19710.